Astronomy & Astrophysics manuscript no. 5204
February 5, 2008

Ionization structure in the winds of B[e] supergiants

II. Influence of rotation on the formation of equatorial hydrogen neutral zones

Michaela Kraus[1,2]

[1] Astronomický ústav, Akademie věd České republiky, Fričova 298, 251 65 Ondřejov, Czech Republic
e-mail: kraus@sunstel.asu.cas.cz
[2] Sterrekundig Instituut, Universiteit Utrecht, Princetonplein 5, 3584 CC Utrecht, The Netherlands

Received / accepted

ABSTRACT

Context. B[e] supergiants are known to have non-spherical winds, and the existence of disks that are neutral in hydrogen close to their stellar surface has been postulated. A suitable mechanism to produce non-spherical winds seems to be rapid rotation, and at least for three B[e] supergiants in the Magellanic Clouds rotation velocities at a substantial fraction of their critical velocity have been found.
Aims. We want to find suitable recombination distances in the equatorial plane of rapidly rotating stars that explain the observed huge amounts of neutral material in the vicinity of B[e] supergiants.
Methods. We perform ionization structure calculations in the equatorial plane around rapidly rotating luminous supergiants. The restriction to the equatorial plane allows us to treat the ionization balance equations 1-dimensionally, while the stellar radiation field is calculated 2-dimensionally, taking into account the latitudinal variation of the stellar surface parameters. The stellar parameters used correspond to those known for B[e] supergiants. The assumptions made in the computations all have in common that the total number of available ionizing photons at any location within the equatorial plane is overestimated, resulting in upper limits for the recombination distances.
Results. We find that despite the drop in equatorial surface density of rapidly rotating stars (neglecting effects like bi-stability and/or wind compression), hydrogen and helium recombine at or close to the stellar surface, for mass loss rates $\dot{M} \gtrsim 5 \times 10^{-5} \mathrm{M}_{\odot}\mathrm{yr}^{-1}$ and rotation speeds in excess of $v_{\mathrm{rot,eq}}/v_{\mathrm{crit}} \simeq 0.8$.

Key words. Stars: rotation – Stars: mass-loss – Stars: winds, outflows – supergiants

1. Introduction

In a series of papers Maeder & Meynet discussed the importance and the influence of rapid rotation on the evolution of stars, the chemical yields and non-spherical mass and angular momentum loss (see e.g Maeder, 1999; Meynet & Maeder, 2000; Maeder & Meynet, 2000). The influence of rotation on so many stellar parameters results also in the shaping of the wind and the nebula. There has been the suggestion that the appearance of non-spherical winds around some massive and luminous stars might be caused by rotation (Maeder 2002; Maeder & Desjacques 2001). Stars for which this might be appropriate are the Luminous Blue Variables and the B[e] supergiants.

Zickgraf et al. (1985) suggested that the hybrid character of the optical spectra of B[e] supergiants is due to a non-spherical (two-component) wind. The strong infrared excess indicates the presence of a huge amount of hot circumstellar dust, and polarimetric observations, e.g. by Magalhães (1992), Magalhães et al. (2006), and Melgarejo et al. (2001), confirmed the non-spherical geometry of the circumstellar material around B[e] supergiants. The existence of a geometrically thick circumstellar disk responsible for the polarized emission and the location of the hot dust seems nowadays to be well established (for an overview see e.g. Kraus & Miroshnichenko 2006). The formation mechanism of these disks is, however, still rather unclear. There exist two promising approaches: (1) the bi-stability mechanism introduced by Lamers & Pauldrach (1991) and further investigated, especially with respect to the influence of rotation on the formation of B[e] supergiant stars' disks, by Pelupessy et al. (2000), and (2) the wind-compressed disk, introduced by Bjorkman & Cassinelli (1993). Both models however have difficulties in explaining *all* observed quantities of the B[e] supergiants' disks in a self-consistent way. In addition, there is still no consensus about the nature of these disks, whether they can be described by a high density equa-

Send offprint requests to: M. Kraus,
e-mail: kraus@sunstel.asu.cas.cz

torial outflowing wind or by a Keplerian viscous disk (see e.g. Porter 2003; Kraus & Miroshnichenko 2006).

Recently, these disks have been suggested to be neutral in hydrogen in the vicinity of the stellar surface. Tracers for hydrogen neutral material are e.g. the strong [OI] emission lines arising in the optical spectra of B[e] supergiants. Modeling of their line luminosities revealed that, in order to keep the mass loss rate of the star at a reliable value, these lines must originate within a few stellar radii from the surface (Kraus & Borges Fernandes 2005; Kraus et al. 2006). In addition, several B[e] supergiants are found to show band-head emission from hot (3000 - 5000 K) CO gas (McGregor et al. 1988). Follow-up studies of high-resolution spectra for at least one of them led to the conclusion that this hot CO gas is located at about 2-3 AU from the hot stellar surface (Kraus 2000; Kraus et al. 2000). The existence of neutral material close to these luminous B[e] supergiants is surprising and needs to be investigated in detail. The goal of our study is therefore to find scenarios that allow neutral material to exist close to the surface of these stars.

In a first attempt, Kraus & Lamers (2003, hereafter Paper 1) calculated the ionization structure of B[e] supergiants, assuming a latitude–dependent mass flux that increases from pole to equator. With such a model they could show that, even with moderate total mass loss rates, hydrogen recombines in the equatorial direction close to the star leading to a hydrogen neutral disk-like structure. Here, we investigate the influence of rotation on the stellar parameters and consequently on the ionization structure in the winds and disks of B[e] supergiants.

Rotation causes a flattening of the stellar surface and therefore a reduction of the local net gravity in the equatorial region. The decrease in gravity from pole to equator equally results in a decrease of the stellar flux which is proportional to the local net gravity. Hence, the effective temperature also decreases from pole to equator, known as gravity darkening (or polar brightening, von Zeipel 1924). The latitude dependence of the gravity and effective temperature has also impacts on the stellar wind parameters (see e.g. Lamers & Cassinelli 1999): The escape velocity following from the balance between gravitational and centripetal forces becomes latitude–dependent, decreasing from pole to equator. The same holds for the terminal wind velocity which is (for line-driven winds) proportional to the escape velocity. Even the mass flux from the star tends to decrease from pole to equator if gravity darkening is taken into account in the CAK theory as shown by Owocki et al. (1998). More important for the ionization structure calculations is the density in the wind, and we will show in Sect. 2 that the density at any given distance also *decreases* from pole to equator. A rotating star will therefore have a less dense wind in the equatorial region, unless special effects such as bi-stability or wind compression play a role.

Both important parameters in the ionization balance equations, i.e. the effective surface temperature *and* the surface density, decrease from pole to equator. While the decrease in surface temperature tends to decrease the number of available photons suitable to ionize H and He, the decrease in surface density reduces the optical depth along the line of sight from a point in the wind to the star. Both effects are therefore counteracting with respect to the location where recombination takes place. While a reduction of ionizing photons will shift the recombination distance towards the star, the reduction in optical depth along the direction to the star will shift it further outwards. The outcome of the ionization balance equations is therefore unpredictible and very sensitive to the chosen input parameters. We thus investigate the ionization structure in the wind of a rotating star in more detail.

The paper is structured as follows: In Sect. 2 we provide the equations that describe the surface distribution of the effective temperature, mass flux, escape velocity (and hence terminal wind velocity), and hydrogen density for a rigidly rotating star. The ionization structure calculations restricted to the equatorial plane of the systems are performed in Sect. 3 where also the results for the recombination distances of helium and hydrogen are shown. The influence of the assumptions on these results and the applicability of the models to B[e] supergiants are discussed in Sects. 4 and 5, respectively, and the conclusions are given in Sect. 6.

2. The surface and wind structure of rigidly rotating stars

In this paper, we restrict our investigations to rigid rotation only, and we neglect any influences due to bi-stability and wind-compression.

2.1. The shape of the stellar surface

The potential Φ of a rotating star is given by the sum of gravitational and centrifugal potential. The latitude dependence of the stellar radius, $R(\theta)$, i.e. the shape of the star, is determined by the equipotential surfaces, $\Phi(R(\theta), \theta, \phi)$, for which it is assumed that all the mass is concentrated in the core. These equipotential surfaces are given by

$$\Phi(R(\theta), \theta, \phi) = -\frac{GM_{\rm eff}}{R(\theta)} - \frac{1}{2}R^2(\theta)\Omega^2 \sin^2(\theta) \quad (1)$$

where θ is the co-latitude with $\theta = 0$ at the pole, $M_{\rm eff}$ is the effective stellar mass, i.e. the stellar mass reduced by the effects of radiation pressure due to electron scattering, and Ω is the angular velocity. With the definitions of $x(\theta) = R(\theta)/R_{\rm eq}$, $v_{\rm crit} = \sqrt{(GM_{\rm eff})/R_{\rm eq}}$, and $\omega = v_{\rm rot,eq}/v_{\rm crit}$, the latitude–dependent stellar radius is found from Eq. (1) which results in the following cubic function

$$x^3 - \frac{2+\omega^2}{\omega^2 \sin^2\theta}\, x + \frac{2}{\omega^2 \sin^2\theta} = 0 \quad (2)$$

with the solution

$$x(\theta = 0) = \frac{R_{\rm pole}}{R_{\rm eq}} = \left(1 + \frac{1}{2}\omega^2\right)^{-1} \quad (3)$$

and

$$x(\theta \neq 0) = 2\frac{\sqrt{2+\omega^2}}{\sqrt{3}\omega \sin\theta}\, \sin\left\{\frac{1}{3}\arcsin\left(\frac{3\sqrt{3}\omega\sin\theta}{(2+\omega^2)^{3/2}}\right)\right\}. \quad (4)$$

Equations (3) and (4) describe the stellar radius at all latitudes for a star rotating rigidly with a specific value of ω.

2.2. The latitude–dependent surface temperature

Rotation not only influences the radius of the star but also results in a latitude–dependent surface temperature distribution, because the stellar flux, F, is proportional to the local effective gravity, $g_{\rm eff}$, which is calculated from

$$g_{\rm eff} = -\nabla\Phi \sim \frac{1}{R^2(\theta)}\left(1 - \frac{R^3(\theta)}{R^3_{\rm eq}}\omega^2 \sin^2\theta\right). \quad (5)$$

Since $F(\theta) = \sigma T^4_{\rm eff}(\theta) \sim g_{\rm eff}$, the surface temperature $T_{\rm eff}(\theta)$ behaves as

$$T^4_{\rm eff}(\theta) \sim \frac{1}{R^2(\theta)}\left(1 - \frac{R^3(\theta)}{R^3_{\rm eq}}\omega^2 \sin^2\theta\right) \quad (6)$$

or, if we express the latitude–dependent effective temperature in terms of the polar temperature, $T_{\rm eff}$(pole), replace $R(\theta)$ by $x(\theta)$, and make use of relation (3),

$$\begin{aligned} T^4_{\rm eff}(\theta) &= T^4_{\rm eff}({\rm pole})\frac{R^2({\rm pole})}{R^2(\theta)}\left(1 - \frac{R^3(\theta)}{R^3_{\rm eq}}\omega^2 \sin^2\theta\right) \\ &= T^4_{\rm eff}({\rm pole})\frac{1}{x^2(\theta)}\frac{(1 - x^3(\theta)\omega^2 \sin^2\theta)}{(1 + \frac{1}{2}\omega^2)^2}. \end{aligned} \quad (7)$$

For the purpose of our paper it is important to treat the surface effective temperature (as well as all other following parameters) properly, which means that we have to take into account the rotationally distorted stellar surface. How different the results can be when accounting only for gravity darkening but neglecting the real shape of the star is shown in Fig. 1. There we compare the surface temperature distribution calculated from Eq. (7) which accounts for the distorted surface with the one resulting from a rotating star but under the assumption of an unperturbed, spherical surface (i.e. $R(\theta) = R_{\rm eq} = R$). In this latter case, $T_{\rm eff}(\theta)$ resulting from Eq. (6) is simply given by (see e.g. Lamers & Cassinelli 1999; Lamers[1] 2004)

$$T^4_{\rm eff}(\theta) = T^4_{\rm eff}({\rm pole})\left(1 - \omega^2 \sin^2\theta\right). \quad (8)$$

This equation also describes globally the influence of rigid rotation, i.e. the drop in temperature from pole to equator. However, the absolute value of the effective temperature at any location on the stellar surface is different, as is obvious from the comparison in Fig. 1:

- For $\omega \lesssim 0.8$ the rotationally distorted surface is cooler at all latitudes.
- For $\omega \gtrsim 0.8$ the effective temperature of the rotationally distorted surfaces is higher for small to intermediate latitudes, but becomes (much) lower in the equatorial regions, compared to the corresponding spherical surfaces.

These severe differences in surface temperature distribution have non-negligible effects on the stellar radiation field at any point in the wind. A proper treatment of the stellar parameters by accounting for the rotationally distorted surface is therefore an important ingredient in our ionization balance calculations.

[1] Please note the typo in Lamers' Eq. (5) where it should be $\cos^2(\theta)$ instead of $\cos(\theta)$, and that in his paper θ is measured from the equator.

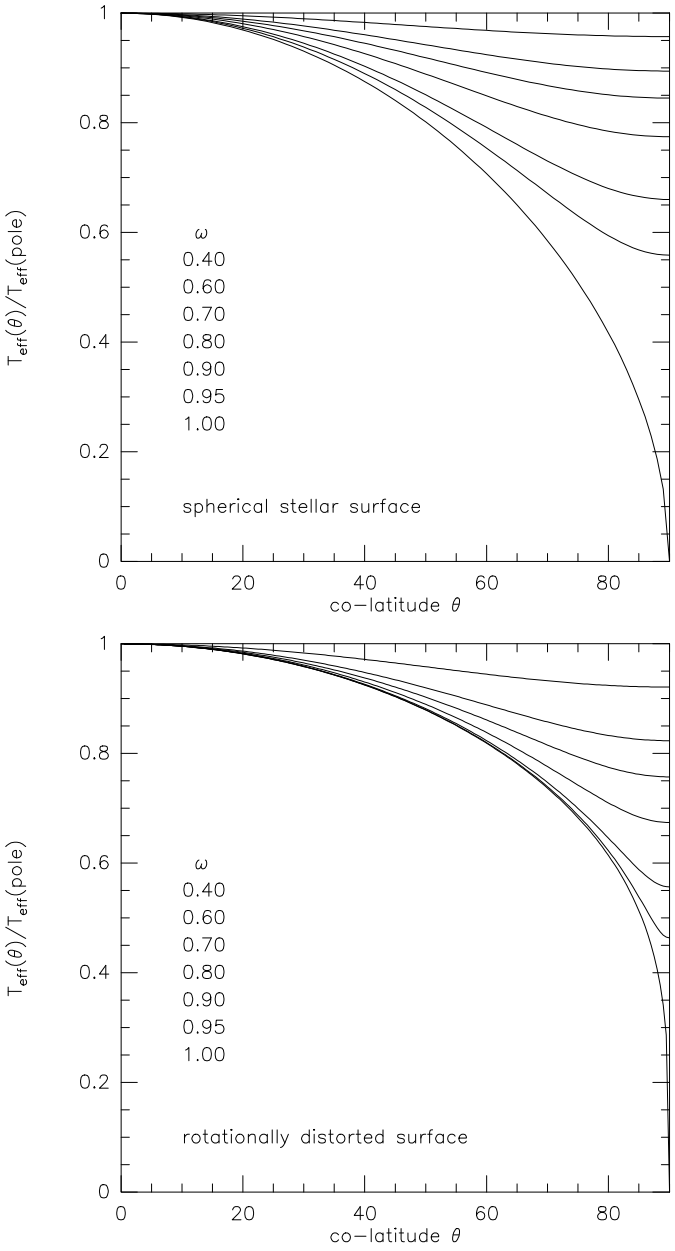

Fig. 1. Effective temperature distribution on the surface of a rotating star. The different curves, which are normalized to the polar temperature, are for different rotational velocities indicated by ω from low values (upper curves) to high values (lower curves). In the top panel the rotational distortion of the stellar surface has been neglected.

2.3. The latitude–dependent mass flux

For the mass flux, $F_{\rm m}$ we follow the description of Owocki et al. (1998) given by their Eq. (2)

$$\frac{F_{\rm m}(\theta)}{F_{\rm m}({\rm pole})} = \left[\frac{F(\theta)}{F({\rm pole})}\right]^{\frac{1}{\alpha}}\left[\frac{g_{\rm eff}(\theta)}{g_{\rm eff}({\rm pole})}\right]^{1-\frac{1}{\alpha}}. \quad (9)$$

This equation describes the latitude–dependent mass flux according to CAK theory (Castor et al. 1975). Neglecting bistability effects, which means that the force multiplier α is constant all over the surface, and introducing gravitational darken-

ing according to the von Zeipel theorem (i.e. $F(\theta) \sim g_{\rm eff}(\theta)$) results in

$$\frac{F_{\rm m}(\theta)}{F_{\rm m}({\rm pole})} = \frac{g_{\rm eff}(\theta)}{g_{\rm eff}({\rm pole})} = \frac{1}{x^2(\theta)} \frac{(1 - x^3(\theta)\omega^2 \sin^2\theta)}{(1 + \frac{1}{2}\omega^2)^2} . \quad (10)$$

The surface distribution of the mass flux for different values of ω is shown in the top panel of Fig. 2.

2.4. The latitude–dependent terminal velocity

The escape velocity of a rotating star follows from balancing gravitational and centripetal forces on the stellar surface which means that the effective gravity $g_{\rm eff}(\theta)$ must equal $v_{\rm esc}^2(\theta)/R(\theta)$. Since the terminal wind velocity, v_∞, is, according to line-driven wind theories (see e.g. Lamers & Cassinelli 1999, Chapter 8), proportional to the escape velocity, $v_{\rm esc}$, we find the following relation for the latitude dependence of the terminal velocity

$$v_\infty(\theta) = v_\infty({\rm pole}) \frac{\left(1 - x^3(\theta)\omega^2 \sin^2\theta\right)^{1/2}}{\left(x(\theta)(1 + \frac{1}{2}\omega^2)\right)^{1/2}} . \quad (11)$$

The latitude dependence of the terminal velocity for different values of ω is shown in the middle panel of Fig. 2.

2.5. The latitude–dependent wind density distribution

It is known that the mass flux and the terminal velocity decrease from pole to equator, even if the rotational distortion of the stellar surface is neglected in their derivation (see Lamers & Cassinelli 1999). For the ionization structure calculations, however, we need to know the density distribution in the wind.

In a non-rotating, spherically symmetric stationary wind, the density at any location r in the wind is related to the mass loss rate, $\dot{M}$, of the star and the wind velocity, $v(r)$, via the equation of mass continuity

$$n_{\rm H}(r) = \frac{\dot{M}}{4\pi\mu m_{\rm H} r^2 v(r)} = \frac{F_{\rm m}}{\mu m_{\rm H} v(r)} \frac{R_*^2}{r^2} \quad (12)$$

where μ is the mean molecular weight and $n_{\rm H}$ denotes the particle density of hydrogen given in cm^{-3}. From the right-hand side of this equation it follows immediately that in a non-spherically symmetric wind, the radial density distribution at any latitude can be written in the form

$$n_{\rm H}(\theta, r) = \frac{F_{\rm m}(\theta)}{\mu m_{\rm H} v(\theta, r)} \frac{R^2(\theta)}{r^2} . \quad (13)$$

For our further calculations, we assume that the wind velocity is constant in radial direction, i.e. $v(\theta, r) = v(\theta, R) = v(\theta)$. Therefore we can re-write Eq. (13) in the form

$$n_{\rm H}(\theta, r) = n_{\rm H}(\theta, R(\theta)) \frac{R^2(\theta)}{r^2} \quad (14)$$

where

$$n_{\rm H}(\theta, R(\theta)) = \frac{F_{\rm m}(\theta)}{\mu m_{\rm H} v(\theta)} \quad (15)$$

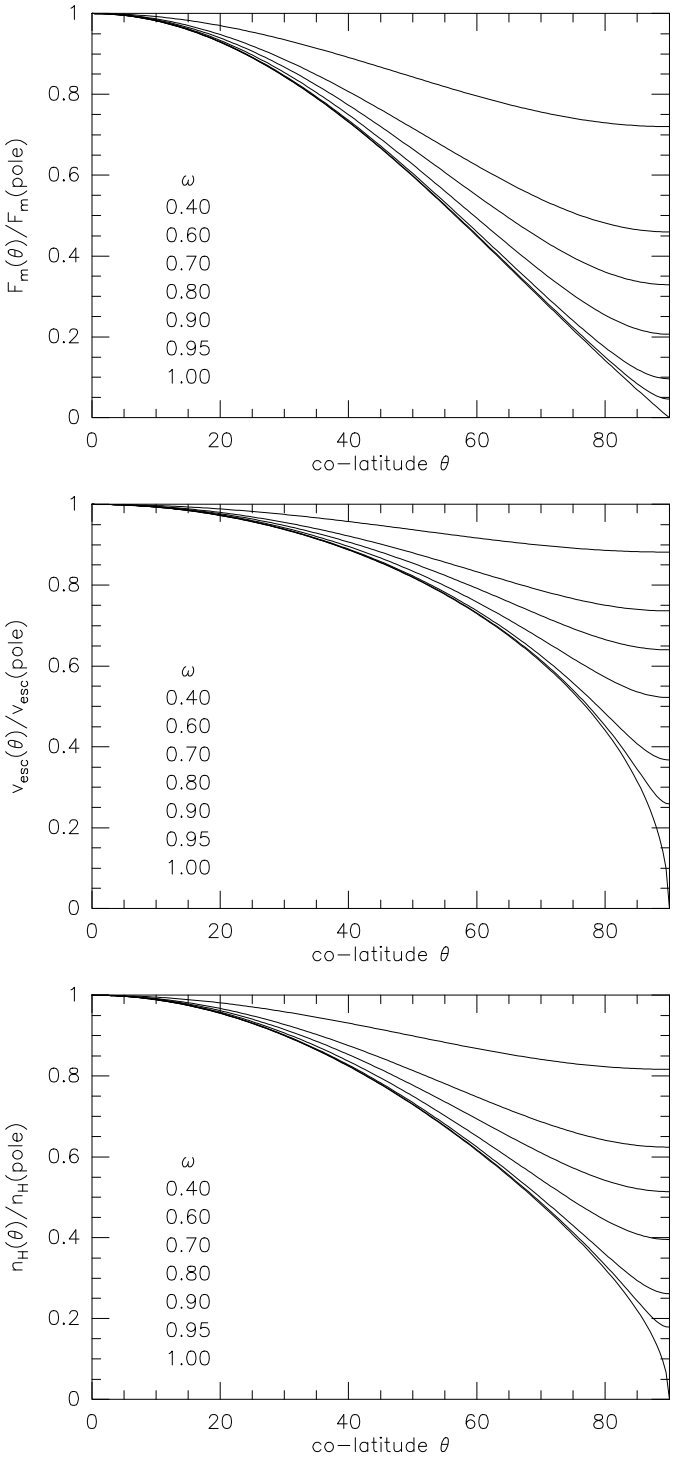

Fig. 2. Distribution of the mass flux (top panel), the escape velocity (mid panel), and the hydrogen density (bottom panel) on the surface of a rotating star. The different curves in each plot, which are normalized to the corresponding polar value of the parameters, are for different rotational velocities indicated by ω. All parameters drop from pole to equator. This effect becomes stronger with increasing values of ω.

defines the density distribution along the stellar surface.

With the additional simplification of $v(\theta) = v_\infty(\theta)$, we can express the surface density distribution, $n_{\rm H}(\theta, R(\theta))$, by using

the relations for the mass flux given by Eq. (10) and for the terminal velocity given by Eq. (11)

$$n_{\rm H}(\theta, R(\theta)) = \frac{F_{\rm m}({\rm pole})}{\mu m_{\rm H} v_\infty({\rm pole})} \frac{\left(1 - x^3(\theta)\omega^2 \sin^2\theta\right)^{1/2}}{\left(x(\theta)(1+\frac{1}{2}\omega^2)\right)^{3/2}} \quad (16)$$

$$= n_{\rm H}({\rm pole}) \frac{\left(1 - x^3(\theta)\omega^2 \sin^2\theta\right)^{1/2}}{\left(x(\theta)(1+\frac{1}{2}\omega^2)\right)^{3/2}} . \quad (17)$$

This surface density distribution, as the result of the ratio of mass flux to terminal velocity, is plotted for different values of ω in the lower panel of Fig. 2. It also decreases from pole to equator. This means that a rigidly rotating star will have a *less dense wind* in the equatorial region, unless bi-stability and wind compression play a role.

3. Ionization structure calculations

Since we are searching for the existence of a hydrogen neutral equatorial region, we restrict our calculations to the equatorial plane only. This leads to the simplification of a symmetrical stellar radiation field with respect to the equatorial plane. Therefore, it is sufficient to solve the ionization balance equations along one radial direction, which we will call the *y*-axis.

As in Paper 1, our model wind consists of hydrogen and helium, only. This means that we have to solve two coupled ionization balance equations that are treated in the on-the-spot (OTS) approximation. This approximation states that every photon generated via recombination and able to ionize hydrogen or helium will be absorbed immediately in the close vicinity of its generation location. The ionization balance equations for this case are given in Sect. 4. of Paper 1. The recombination distance is found by applying a root-finding routine. Usually, a few iteration steps are sufficient for an accuracy in distance better than 1%.

3.1. The stellar radiation field

Besides the OTS approximation, which defines the diffuse radiation field, we need to calculate the stellar radiation field at any point in the equatorial plane, or, due to the symmetry in our case, at any point along the *y*-axis. Differently from the treatment in Paper 1 we no longer use the assumption that the star is a point source. The stellar parameters of a rotating star vary strongly over the stellar surface, especially for increasing stellar rotation. We therefore calculate the stellar radiation by integrating the latitude–dependent surface flux over the rotationally distorted stellar surface. This is done in the following way:

- We define the stellar input parameters $T_{\rm eff}$(pole), $g_{\rm eff}$(pole), v_∞(pole), R_*(sphere), $F_{\rm m}$(pole).
- We define the rotation velocity, ω.
- With ω and R_*(sphere) we calculate the shape of the stellar surface, i.e. $x(\theta)$. We thereby make use of Eq. (3) and of the mass conservation that relates the spherical radius to the equatorial and polar radii via $R_*^3 = R_{\rm eq}^2 R_{\rm pole}$.
- At each location r along the *y*-axis we determine the angular extent of the stellar surface and its shape. This defines the size of the stellar surface (or the surface segment) from which radiation will arrive at point r.
- Along this stellar surface segment we calculate the distribution of $T_{\rm eff}(\theta)$ and $g_{\rm eff}(\theta)$, and the resulting radiation temperature $T_{\rm rad}(\theta)$ (see Sect. 3.2).
- The stellar flux as a function of latitude is then approximated by $B_\nu(T_{\rm rad}(\theta))$.
- The total stellar radiation field at point r along the *y*-axis follows from integration of $B_\nu(T_{\rm rad}(\theta))$ over the segment of the rotationally distorted surface.
- To account for optical depth effects, we calculate the *minimum* optical depth, which occurs along the *y*-axis (because of the shortest distance and the lowest density). This optical depth is adopted for all directions towards the stellar surface.

In this calculation of the stellar radiation field at any point r along the *y*-axis we make one important approximation, which is the adoption of the minimum optical depth towards all directions from r to the stellar surface. This assumption results in an overprediction of the available ionizing photons, because the stellar radiation from the higher latitudes with higher $T_{\rm eff}$ will be absorbed less. The resulting recombination distance will therefore be overestimated.

3.2. The radiation temperature

The stellar radiation temperature is defined in our calculations as the Planck temperature which describes the part of the stellar spectrum that delivers the ionizing photons, i.e. the spectrum shortwards of 912 Å. The determination of the latitude dependence of the radiation temperature is not straightforward. We therefore briefly explain how we calculate it.

We start with Kurucz model atmospheres (Kurucz 1979) for solar metallicity stars and $\log g$ values between 2.0 and 3.5. We do not investigate higher values of $\log g$ because we are mainly interested in giants and supergiants. For each model atmosphere in this $\log g$ range and for all available effective temperatures we fitted a Planck function to the spectrum shortwards of 912 Å. This delivers the radiation temperature for the corresponding ($T_{\rm eff}$, $g_{\rm eff}$) combination. The radiation temperature is therefore a function of these two parameters, i.e. $T_{\rm rad} = T_{\rm rad}(T_{\rm eff}, g_{\rm eff})$, and we found the following useful parametrization:

$$\log T_{\rm rad} = A(\log g)\ \log T_{\rm eff} + B(\log g) \quad (18)$$

with the two functions $A(\log g)$ and $B(\log g)$ given by

$$A(\log g) = 1.222 - 0.058 \log(\log g - 1.9) \quad (19)$$

$$B(\log g) = 0.235 \log(\log g - 1.89) - 1.13 \quad (20)$$

in the range of $8\,000 \lesssim T_{\rm eff} \lesssim 30\,000$ K. The error in radiation temperature introduced by this fitting procedure is less than 5% for the higher values of $T_{\rm eff}$, and less than 3% for the lower ones. We thus can compute $T_{\rm rad}(\theta)$ for any combination of $T_{\rm eff}$ and $g_{\rm eff}$ values that will occur along the surface of a rigidly

rotating star, and hence we can calculate the appropriate stellar radiation at all locations on the stellar surface.

Since $T_{\rm rad}(\theta)$ is a function of both $T_{\rm eff}$ and $g_{\rm eff}$, its latitude dependence will be different from the one of the effective temperature (see Sect. 3.4), and will also vary for stars with different stellar parameters.

3.3. Description of the model stars and their winds

For our calculations we chose stars with a polar effective temperature of $T_{\rm eff,pole} \simeq 24\,500\,{\rm K}$ and $\log g_{\rm eff,pole} = 3.5$. According to Eq. (18) this combination results in a polar radiation temperature of $T_{\rm rad,pole} \simeq 17\,000\,{\rm K}$.

The radius of the non-rotating star is fixed at $R_* = 82\,{\rm R}_\odot$. Together with the chosen effective temperature this results in a luminosity of the non-rotating star of $L_* \simeq 2.2 \times 10^6\,{\rm L}_\odot$, which places the star in the B-type supergiant region within the HR diagram.

The polar values of the effective temperature and gravity (and hence radiation temperature) are fixed for all our model calculations. Fixing the polar effective temperature means that we are *not* calculating a star that is spinning up. This would result in an increase of polar temperature with increasing rotation velocity. Instead, we are calculating stars with the same polar effective temperature having different rotation velocities. This means that we are dealing with stars of *different luminosities*. The total luminosity of a star is

$$L_* = \int_0^{\pi} \int_0^{2\pi} \sigma T_{\rm eff}^4(\theta)\, dS \qquad (21)$$

where dS is the surface element of an ellipsoid, given by

$$dS = \sqrt{(R_{\rm eq}^2 \cos^2\theta + R_{\rm pole}^2 \sin^2\theta)}\ R_{\rm eq} \sin\theta\, d\theta\, d\phi\ . \qquad (22)$$

The difference in luminosity of rotating stars having the same polar effective temperature is shown in the upper panel of Fig. 3 where we plotted the distribution of the stellar luminosities as a function of ω. With increasing rotation speed, the stellar luminosity drops. The difference is largest between the non-rotating and the critically rotating star, and is about a factor 2.

Similarly, we can calculate the mass loss rates of our model stars. The mass loss rate follows from

$$\dot{M}_* = \int_0^{\pi} \int_0^{2\pi} F_{\rm m}(\theta)\, dS \qquad (23)$$

and the ratio of the mass loss rate over the mass loss rate of the spherical star is plotted as a function of ω in the lower panel of Fig. 3. The mass loss rate shows a difference of about a factor 2 between the non-rotating and the critically rotating star. The behaviour of both the luminosity and the mass loss rate with ω is identical because both $T_{\rm eff}^4(\theta)$ and $F_{\rm m}(\theta)$ are proportional to $g_{\rm eff}(\theta)$ (see Eqs. (7) and (10) respectively). We can therefore conclude that an almost critically rotating star will have only half the total luminosity and half the total mass loss rate of its non-rotating counterpart, having both the same polar mass flux and effective temperature.

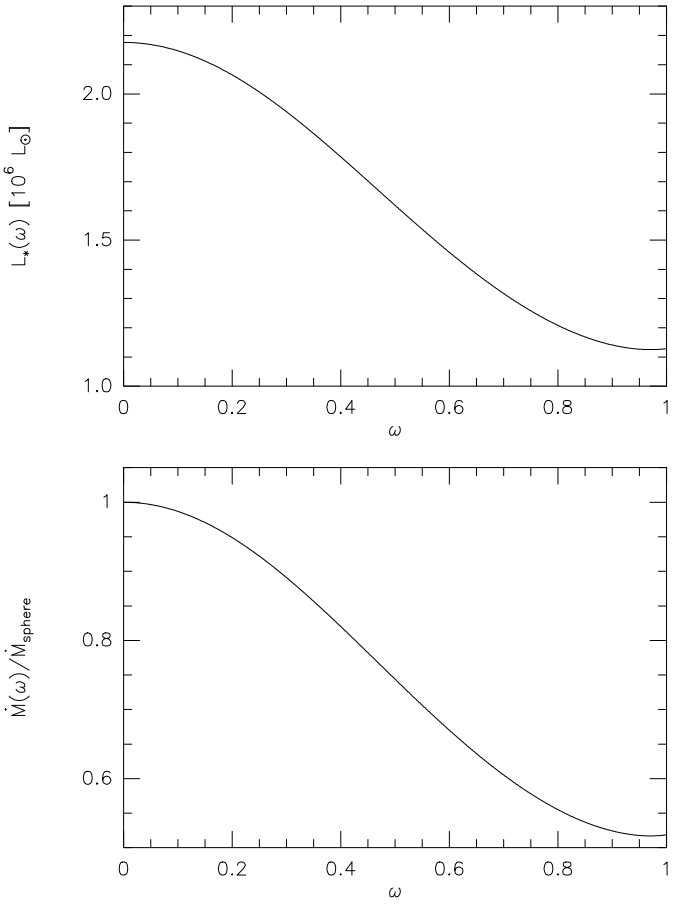

Fig. 3. Top panel: Stellar luminosity as a function of ω for our model stars with $T_{\rm eff,pole} = 24\,500\,{\rm K}$ and $R_* = 82\,R_\odot$. Bottom panel: Mass loss rate as a function of ω, normalized to the spherical mass loss rate. Both parameters show a decrease with increasing rotation speed. The difference between the non-rotating and the critically rotating star is about a factor 2.

In our calculations, the polar mass flux, $F_{\rm m,pole}$, is a free parameter. Its value is varied over a large range to investigate the ionization structure of rotating stars and to find the recombination distances (see Sect. 3.4).

We further use a distant independent wind velocity, which is set to the terminal velocity, i.e. $v(\theta, r) = v_\infty(\theta)$. For the polar wind velocity we adopt $v_{\infty,\rm pole} = 2000\,{\rm km\,s^{-1}}$. The radial electron temperature distribution in the wind is assumed to be constant, and we set $T_{\rm e}(\theta, r) = T_{\rm e}(\theta) = 0.8\,T_{\rm eff}(\theta)$. The influence of these assumptions and simplifications on the results are discussed in Sect. 4.

3.4. Recombination in the equatorial plane

We calculated the equatorial recombination distance of H and He for stars with a large range in polar mass fluxes, $F_{\rm m,pole}$. For each mass flux we considered rotation velocities ω covering the complete range from 0 to 1. In Fig. 4 we show the results of three representative models, calculated for $F_{\rm m,pole} = 1.0 \times 10^{-5}$, 1.5×10^{-5}, and $2.0 \times 10^{-5}\,{\rm g\,s^{-1}cm^{-2}}$. The recombination radii for helium (left panel) and hydrogen (right panel) are given in

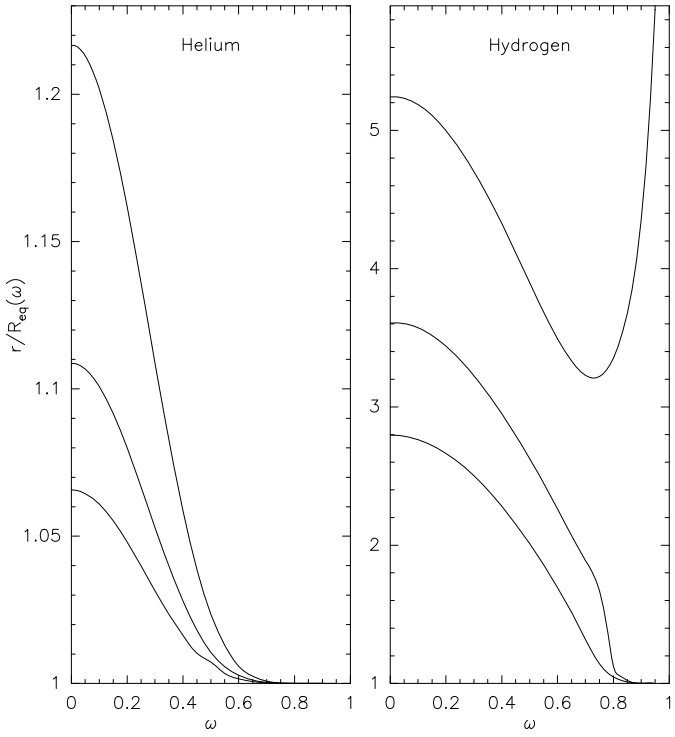

Fig. 4. Distance r in the equatorial plane in terms of the equatorial radius $R_{\rm eq}(\omega)$ at which recombination of HeII (left panel) and HII (right panel) takes place for stars rotating with different velocities, indicated by ω. The curves are (from top to bottom) for polar mass fluxes of: $F_{\rm m}({\rm pole}) = 1.0\times10^{-5}$, 1.5×10^{-5} and $2.0\times10^{-5}\,{\rm g\,s^{-1}cm^{-2}}$.

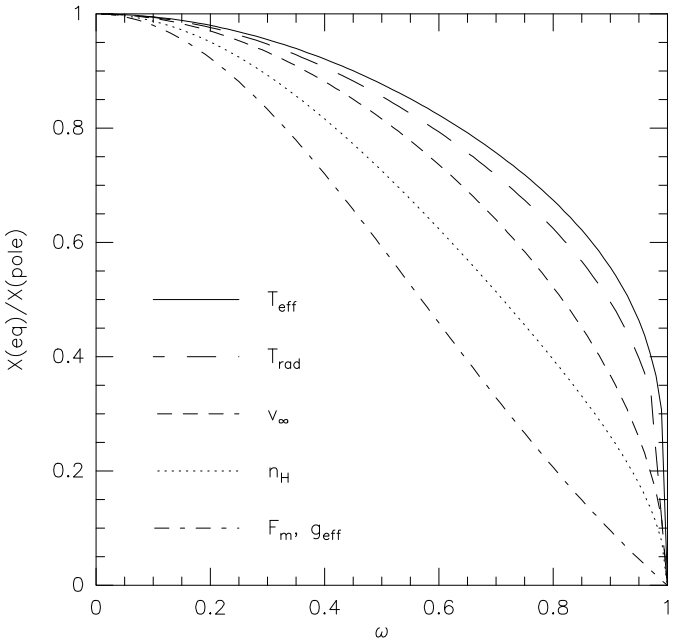

Fig. 5. Surface parameters in the equatorial plane, normalized to their polar values, as functions of the rotational velocity. $n_{\rm H}$ is the density at any distance.

units of the corresponding ω–dependent stellar equatorial radius, $R_{\rm eq}(\omega)$. Helium recombines for all models already close to the stellar surface. The recombination distance is found to decrease steadily with increasing stellar rotation, reaching the stellar surface for $\omega \gtrsim 0.7$. This means that for rapidly rotating stars helium is neutral at the stellar surface. For hydrogen, the situation is different. For polar mass fluxes $F_{\rm m,pole} \lesssim 1.5\times10^{-5}{\rm g\,s^{-1}cm^{-2}}$ the recombination distances decrease with increasing ω, reach a minimum in the range $\omega \simeq 0.70\ldots0.75$, and increase again for higher rotation speeds. If the input polar mass flux is higher than $1.5\times10^{-5}{\rm g\,s^{-1}cm^{-2}}$, hydrogen shows the same trend as helium, i.e. the recombination distances decrease steadily for increasing stellar rotation. They reach also the surface of the star, but for rotation speeds $\omega \gtrsim 0.85$. The models with $F_{\rm m,pole} = 1.5\times10^{-5}{\rm g\,s^{-1}cm^{-2}}$ seem to be the case in "transition". They show a kink at $\omega = 0.75$ and a subsequent steep drop in recombination distance.

What causes the minimum and especially the strong increase in hydrogen recombination distance for the lower mass flux models? This rather unexpected behaviour can be understood upon inspection of Fig. 5. There we plotted the variation of the individual equatorial surface parameters with ω, and of special interest are the radiation temperature and the particle density. Fig. 5 shows that with increasing rotation velocity, the density drops much quicker from pole to equator than the temperature. For recombination to take place right above the stellar surface, the number of ionizing photons has to be reduced. This can be done either by decreasing the radiation temperature, or by increasing the equatorial surface density and hence the optical depth. Since the decrease in radiation temperature is determined by the rotation velocity (with a fixed input polar value) we can only increase the input polar mass flux to achieve a higher surface density for a given rotation velocity. A higher density also has the effect of triggering recombination, this is however only a secondary effect while the blocking of the raidation field is the more important one. The density in the top model shown in Fig. 4 is no longer high enough for stars with $\omega \geq 0.7$ to absorb the ionizing photons provided by the still rather high radiation temperature. Therefore, ionization takes over again and shifts the recombination distance for higher rotation velocities further out. Whether recombination takes place close to the star therefore sensitively depends on the chosen input parameters of the rotating star.

4. Discussion

For our calculations we made a few assumptions, and we briely discuss their influence on the model results:

The electron temperature. The winds of hot stars are known to start with an electron temperature of about $0.8\,T_{\rm eff}$ at the stellar surface. Further out, they cool quickly (within a few stellar radii) and converge towards a more or less constant (terminal temperature) value (see e.g. Drew 1989). The adoption of a constant (in radial direction) and maximum (i.e. $T_{\rm e}(\theta, r) = 0.8\,T_{\rm eff}(\theta)$) electron temperature reduces (or suppresses) the total number of recombinations taking place, because the recombination coefficient is small for high temperatures but increases with decreasing temperature (see Fig. 2 in Paper 1). Our assumption therefore inhibits recombination and shifts the equilibrium of the ionization balance in favour of the

ionization of the wind material. This means that we have overestimated the recombination distance.

The wind velocity. The velocity distribution in winds of hot stars can usually be approximated by a β-law (see e.g. Lamers & Cassinelli 1999) which describes the increase in velocity from the small surface value to the terminal velocity. First, using the maximum (i.e. terminal) velocity instead of the more realistic β-law increasing velocity distribution results in an underestimation of the density, especially at distances close to the star. Second, the chosen value of 2000 km s^{-1} for the polar terminal velocity is rather high for a B-type supergiant and results equally in an underestimation of the density. Both assumptions therefore lead to an underestimation of the optical depth seen by the stellar radiation and an overestimation of the recombination distance.

The optical depth. We calculate the optical depth properly only along the *y*-axis. Since the surface density of a rotating star drops from pole to equator and since the distance from the stellar surface to any point along the *y*-axis is the shortest one over which stellar photons can be absorbed, this optical depth value is the smallest. Adopting this minimum optical depth for all directions towards the stellar surface therefore underestimates the real optical depth and allows more ionizing photons to penetrate the wind material to larger distances. This leads to an overestimation of the recombination distance.

The OTS approximation. In the OTS approximation it is assumed that every photon created via recombination and able to (re-)ionize hydrogen or helium will be absorbed in the close vicinity of its generation location, and none will escape from the wind. These leads to additional ionizing photons (better known as the diffuse radiation field) at any location in the wind. The OTS approximation, even if not fully applicable for the lower density regions, tends to overestimate the number of available photons everywhere in the wind and therefore favours the ionization of the wind material.

All these assumptions and simplifications made in our computations and listed here show the tendency to overestimate the number of ionizing photons available at a certain location in the wind. Consequently, the recombination radius is shifted away from the star which means that our calculated distances at which the material is found to recombine are *upper limits*.

5. Applicability to the B[e] supergiants

In Sect. 3.4 we showed that the equatorial winds of rapidly rotating stars might be neutral in hydrogen right from the stellar surface, even though the density in the equatorial wind is much lower than in the polar regions. Since our main goal is to find possible formation mechanisms for hydrogen neutral disks around B[e] stars and especially B[e] supergiants, we discuss here how reliable the results are and whether they are indeed applicable to the known B[e] supergiants.

The rotation velocities of B[e] supergiants. Our model is based on the assumption that B[e] supergiants are rapidly rotating stars. What is the evidence for their rapid rotation? In fact not much is known about their rotation velocities. Due to their high density circumstellar medium, most of them do not show any photospheric absorption lines which might be used to derive a possible rotation speed. There are, however, three (out of 15) B[e] supergiants in the Magellanic Clouds for which photospheric absorption lines have been detected. From these line profiles only the projected stellar rotation (i.e. $v \sin i$) can be derived with high accuracy. With their (often) poorly known inclinations i, only *lower limits* to the real rotation speeds could be derived. These were found to be $\omega > 0.35$ and $\omega > 0.45$ for the two LMC B[e] supergiants Hen S93 and R 66 (Gummersbach et al. 1995; Zickgraf 2006, respectively), and $\omega \simeq 0.8$ for the SMC B[e] supergiant R 50 (Zickgraf 2000). Especially the latter seems to rotate at a substantial amount of its critical velocity providing the basis for our research, although we cannot generalize that all B[e] supergiants are rapidly rotating.

Stellar luminosities and effective temperatures. A summary of the stellar parameters ($T_{\rm eff}$, L_*, R_*) of the MC B[e] supergiants is given e.g. in Zickgraf (2006). From this list it is obvious that the stellar luminosities and effective temperatures of the B[e] supergiants cover the range $10^4 \lesssim \log L/L_\odot \lesssim 10^6$ and $10\,000 \lesssim T_{\rm eff}[{\rm K}] \lesssim 27\,000$, and our chosen values of the effective temperature fall well into this range while our luminosities are taken as maximum values. The literature values for the B[e] supergiant effective temperatures, however, should be taken with caution because they have mainly been derived from fitting Kurucz model atmospheres to the observed spectral energy distributions (see Zickgraf 1998 and references therein). However, these model atmospheres have been calculated under the assumption of spherically symmetric, non-rotating (i.e. uniformly bright) stars. If B[e] supergiants are indeed rapidly rotating, then for a proper determination of the mean (i.e. observable) effective temperature a comparison with composite spectra should be undertaken (see e.g. Lovekin et al. 2006). Of course, to do so the inclination and the rotational velocities must be known which is usually not the case for B[e] supergiants.

Mass loss rates. The models presented in Fig. 4 are for stars with polar mass fluxes between 1.0×10^{-5} and 2.0×10^{-5} g s^{-1}cm^{-2}. Therefore, the range in mass loss rates covered by these calculations extends from $\dot{M}_{\rm min} = 3.4 \times 10^{-5} {\rm M}_\odot {\rm yr}^{-1}$ (critically rotating star with lower polar mass flux) to $\dot{M}_{\rm max} = 1.3 \times 10^{-4} {\rm M}_\odot {\rm yr}^{-1}$ (non-rotating star with higher polar mass flux), and is in good agreement with the known mass loss rates for MC B[e] supergiants, which range from about $10^{-5} {\rm M}_\odot {\rm yr}^{-1}$ to about $10^{-4} {\rm M}_\odot {\rm yr}^{-1}$ (see Zickgraf 2006).

The equatorial surface density. According to Eq. (12), the surface density of a non-rotating star behaves as $n_{\rm H}(R_*) \sim \dot{M}/(R_*^2 v(R_*)) = F_{\rm m}/v(R_*)$. For our model calculations we have chosen mass loss rates in the range reliable for B[e] supergiants, but we used some maximum values for the velocity ($v(R_*) = v_\infty$) and stellar radius[2]. Therefore, for non-rotating stars the surface densities in our calculations provide some lower limits.

For (especially rapidly) rotating stars, the situation becomes more complicated. Now, the surface density is found

[2] There exists one exception in the literature: The (more or less) pole-on LMC star R 66 is assumed to have a radius of 125 $R_\odot$ (see Table 1 in Zickgraf 2006), while all other stars fall well below our adopted radius of 82 $R_\odot$.

to drop from pole to equator. On the other hand, B[e] supergiants are supposed to have circumstellar disks. These disks are much denser than what is found for the polar wind regions, with density contrasts on the order of $\rho_{\rm eq}/\rho_{\rm pole} \simeq 100 \ldots 1000$. Models proposed to explain the formation of these high density disks are the bi-stability mechanism (Lamers & Pauldrach 1991; Pelupessy 2000) and wind compression (Bjorkman & Cassinelli 1993). While the bi-stability mechanism in a rotating star might account for an increase by a factor of ~ 10 in equatorial density only, the wind compression, especially for rapidly rotating stars (or more precisely the flow of material towards the equatorial plane), can be inhibited due to the appearance of a non-radial force provided by the radiation (Owocki et al. 1996). Recently, the existence of a slow solution in line–driven winds of rapidly rotating stars has been found (Curé 2004; Curé et al. 2005). Inclusion of the bi-stability jump resulted in an equatorial density enhancement (at least in the close vicinity of the star) by a factor of 100 – 1000, just what is needed to explain the disks of B[e] supergiants. However, these solutions have been found adopting a spherically symmetric star and neglecting gravity darkening, and it still needs to be confirmed that these slow solutions will also exist when gravity darkening is taken properly into account.

Our models do not account for any density enhancements either due to bi-stability or due to wind compression. Such an increase in equatorial surface density by a factor 100 – 1000 (for the same imput values) would result in a recombination distance even closer to the stellar surface, or would mean that the polar mass flux of the model star can be reduced by the same factor and the material would still recombine in the vicinity of the star. Such a lower mass flux (and hence a lower mass loss rate) might be desirable if the winds of B[e] supergiants are clumped. A clumpy wind in contrast to the assumed smooth density distribution is found to overestimate the mass loss rates (derived e.g. from Hα) by a factor of 10 or more (see e.g. Hillier 2005; Bouret et al. 2005).

Even if the winds of B[e] supergiants will turn out to have lower mass loss rates, the ionization structure calculations presented in this paper show that recombination of the equatorial wind material of rapidly rotating stars can take place at or at least close to the stellar surface.

6. Conclusion

We investigated the influence of rigid rotation on the surface and wind parameters of hot luminous stars, with emphasis on the non-spherical winds of B[e] supergiants. Since B[e] supergiants are known to have equatorial disks that show evidence for hydrogen neutral material in the vicinity of the stellar surface, the calculations are restricted to the equatorial plane. Due to the symmetric stellar radiation field (with respect to the equatorial plane) the problem of finding the recombination distance reduces even to the 1-dimensional case. The radiation field is however treated 2-dimensionally, to properly account for the latitude dependences of the parameters like effective temperature, wind velocity and density. The ionization balance equations are solved in a pure hydrogen plus helium wind. All assumptions made during our calculations have in common that the number of available ionizing photons at any location within the equatorial plane is overestimated. This results in a shift of the recombination distance to larger values, which means that we have calculated *upper limits* for the recombination distance.

The major result is that despite the drop in equatorial surface density with increasing rotation velocity (neglecting any possible equatorial density enhancement due to bi-stability and/or wind compression), hydrogen recombines at (or close to) the stellar surface for rotating models with a polar mass flux $F_{\rm m,pole} \gtrsim 1.5 \times 10^{-5} {\rm g\,s^{-1}cm^{-2}}$ and rotation velocities $\omega \gtrsim 0.8$ (see Fig. 4). These mass fluxes correspond to mass loss rates $\dot{M} \gtrsim 5 \times 10^{-5}\,{\rm M_\odot yr^{-1}}$ for our chosen model stars with supergiant stellar and wind parameters. Since the mass loss rates for B[e] supergiants are found to lie in the range $\dot{M} = 10^{-5} \ldots 10^{-4}\,{\rm M_\odot yr^{-1}}$ we can expect that at least some of these stars might have hydrogen neutral equatorial material close to their stellar surface, given that they are indeed (rapidly) rotating stars, as is found for at least three of them.

Acknowledgements. I am grateful to Henny Lamers for his helpful comments and suggestions and for his proof-reading of the draft of this paper. This research was supported by grants from GA ČR 205/04/1267 and from the Nederlandse Organisatie voor Wetenschappelijk Onderzoek (NWO) grant No. 614.000.310.

References

Bjorkman, J. E., & Cassinelli, J. P. 1993, ApJ, 409, 429
Bouret, J.-C., Lanz, T., & Hillier, D. J. 2006, A&A, 438, 301
Castor, J. I., Abbott, D. C., & Klein, R. I. 1975, ApJ, 195, 157
Curé, M. 2004, ApJ, 614, 929
Curé, M., Rial, D. F., & Cidale, L. 2005, A&A, 437, 929
Drew, J. E. 1989, ApJS, 71, 267
Gummersbach, C. A., Zickgraf, F.-J., & Wolf, B. 1995, A&A, 302, 409
Hillier, D. J. 2005, in ASP Conf. Ser. 332, The Fate of the Most Massive Stars, ed. R. Humphreys & K. Stanek (San Francisco: ASP), 219
Kraus, M. 2000, Modeling of the Near IR Emission from the Peculiar B[e] star MWC 349, PhD thesis, University of Bonn
Kraus, M., & Borges Fernandes, M. 2005, in ASP Conf. Ser. 337, The nature and evolution of disks around hot stars, ed. R. Ignace & K. G. Gayley (San Francisco: ASP), 254
Kraus, M., & Lamers, H. J. G. L. M. 2003, A&A, 405, 165 (Paper 1)
Kraus, M., & Miroshnichenko, A. S. 2006, Stars with the B[e] Phenomenon, (San Francisco: ASP), in press
Kraus, M., Borges Fernandes, M., Andrade Pilling, D., & de Araújo, F.X. 2006, in ASP Conf. Ser., Stars with the B[e] Phenomenon, ed. M. Kraus & A. S. Miroshnichenko (San Francisco: ASP), in press [astro-ph/0511822]
Kraus, M., Krügel, E., Thum, C., & Geballe, T. R. 2000, A&A, 362, 158
Kurucz, R. L. 1979, ApJS, 40, 1
Lamers, H. J. G. L. M., & Cassinelli, J. P. 1999, Introduction to stellar winds (Cambridge University Press)
Lamers, H. J. G. L. M., & Pauldrach, A. W. A. 1991, A&A, 244, L5
Lamers, H. J. G. L. M., 2004, in IAU Symp. No. 215, Stellar Rotation, ed. A. Maeder & P. Eenens (San Francisco: ASP), 479
Lovekin, C. C., Deupree, R. G., & Short, C. I. 2006, ApJ, in press [astro-ph/0602084]
Maeder, A. 1999, A&A, 347, 185

Maeder, A. 2002, A&A, 392, 575
Maeder, A., & Desjaques, V. 2001, A&A, 372, L 9
Maeder, A., & Meynet, G. 2000, A&A, 361, 159
Meynet, G., & Maeder, A. 2000, A&A, 361, 101
Magalhães, A. M. 1992, ApJ, 398, 286
Magalhães, A. M., Melgarejo, R., Pereyra, A., & Carciofi, A. C. 2006, in ASP Conf. Ser., Stars with the B[e] Phenomenon, ed. M. Kraus & A. S. Miroshnichenko (San Francisco: ASP), in press [astro-ph/0602170]
McGregor, P. J., Hillier, D. J., & Hyland, A. R. 1988, ApJ, 334, 639
Melgarejo, R., Magalhães, A. M., Carciofi, A. C., & Rodrigues, C. V. 2001, A&A, 377, 581
Owocki, S. P., Cranmer, S. R., & Gayley, K. G. 1996, ApJ, 472, L115
Owocki, S. P., Cranmer, S. R., & Gayley, K. G. 1998, Ap&SS, 260, 149
Pelupessy, I., Lamers, H. J. G. L. M., & Vink, J. S. 2000, A&A, 359, 695
Porter, J. M. 2003, A&A, 398, 631
von Zeipel, H. 1924, MNRAS, 84, 665
Zickgraf, F.-J. 1998, Non-spherical stellar winds in the post-main sequence evolution of massive stars, Habilitation Thesis, Heidelberg University
Zickgraf, F.-J. 2000, in ASP Conf. Ser. 214, The Be Phenomenon in early-type stars, ed. M. A. Smith, H. F. Henrichs, & J. Fabregat (San Francisco: ASP), 26
Zickgraf, F.-J. 2006, in ASP Conf. Ser., Stars with the B[e] Phenomenon, ed. M. Kraus & A. S. Miroshnichenko (San Francisco: ASP), in press
Zickgraf, F.-J., Wolf, B., Stahl, O., Leitherer, C., & Klare, G. 1985, A&A 143, 421

List of Objects